# To Study of Structural, Magnetic and Dielectric Properties of $Cd^{2+}$ Substituted Nickel Ferrite Oxide ($Ni_{1-X}Cd_xFe_2O_4$) Synthesis by Auto-Combustion Route.

**K.R. Kharat[1], S.L.Jadhav[2] A.A. Bagade[3],A.L.Jadhav[4]* J.L. Bhosale[5], T.S. Magdum[6]***
1. Department of Physics, Prof. Dr. N.D. Patil Mahavidyalaya, Malkapur-415101, India.
2. Department of Physics, D.P.Bhosale College, Koregaon, Satara, 415501, India.
3. Sharad Institute of Technology College of Engineering, Yadrav (Ichalkaranji), 416121, India.
4. Punyashok Aahilyadevi Holkar Solapur University, Kegaon, Solapur, 413255,India.
5. Department of Physics, Shikshanmaharshi Dr. Bapuji Salunkhe College, Miraj-416410, India.
6. Department of Physics, Yashwantrao Chavan Mahavidyalaya, Halkarni-416552, India.

***Abstract :*** In this work cadmium ($Cd^{2+}$) substituted nickel ferrite ($NiFe_2O_4$) were synthesized by simple gel auto-combustion technique. The X-ray diffraction confirms that the samples are polycrystalline with spinel cubic crystal symmetry. The lattice constants increased with increasing $Cd^{2+}$ content which obeys Vegard's law. SEM confirms the highly porous surface with increasing symmetry. The two characteristic absorption bands around 392 and 600 $cm^{-1}$ in infrared spectra confirm characteristic futures of ferrite. Magnetic measurements reveal that the saturation of magnetization decreases with an increase in $Cd^{2+}$ constituent in ferrous oxide. The $Cd^{2+}$ions present in A-site and $Fe^{3+}$ are distributed in both tetrahedral and octahedral sites of spinel lattice. The DC measurement shows that the semiconducting behaviour and the curie temperature decrease with an increase in $Cd^{2+}$ constituent. A dielectric measurement of all samples shows the usual dielectric dispersion with frequency. The impedance spectroscopy analysis suggests grain interior contribution in the conduction process.

***Keywords:*** Ni-Cd ferrite oxide; auto-Combustion; XRD; FT-IR; Dielectric; Magnetic properties

## I. INTRODUCTION

In recent years, the rapid developments of modern high-speed communication technology and electronic devices have been responsible for increasing microwave radiation pollution. Consequently, more and more research has been done on creating microwave absorbing materials. A recent candidate for a microwave absorbing interesting material is nanoparticles of spinel ferrite due to their important magnetic and dielectric properties [1]. In general, microwave absorbing materials describe by two way (a) magnetic materials and (b) dielectric materials. Magnetic materials, particularly ferrites are excellent for microwave absorption due to their unique magnetic properties. The magnetization in spinel ferrite is occurring in spin magnetic moments of unpaired electrons of transition metal cations that are distributed among tetrahedral (A), octahedral (B) sites. The exchanges of spins between tetrahedral (A), octahedral (B) sites are known as superexchange magnetic interaction (SEMI). The Mossbauer spectra involve two independent distinct distributions of effective fields and the relative area of site(A) and Site(B) ferric contributions suggest the existence of reversed magnetic moments located in octahedral sites result observed by Grenche et al. [2].

The nickel ferrite is the low cost soft magnetic material and has significant magnetic and electrical properties. The so many properties of ferrites such as magnetization behaviors, low dielectric losses, Curie temperature, and DC resistivity. These properties are based on the ionic composition of material, heat treatment, and type of substituted ions in the synthesized composite materials. Cd-Ni ferrite oxide has a spinal structure, in which tetrahedral A-sites are of a building by $Cd^{2+}$, $Ni^{2+}$ ions, and octahedral B-sites are of a building by $Fe^{3+}$ ions [3]. The substitution of other metal ions has been commonly used to modify the physicochemical, electrical, and magnetic properties in the ferrite. The structural formula for spinel ferrites is $Ni_{1-x}Cd_xFe_2O_4$ where x is the inversion parameter. For the normal spinel, the inversion parameter is zero and the inverse spinel is one. Several reports show improvement in these properties such as electric, magnetic and dielectric losses of substituted nickel ferrite [4]. Their properties of the ferrite nonmaterial as well depend on the cations distribution and additionally paucity in the chemicals composition [5]. Among all the

ferrites, cadmium substituted nickel ferrite is considered to be the most adaptable and found broad extend purpose in the electronics and microwave absorbing devices due to high electrical resistivity, low eddy current, and shows excellent dielectric loss [6-9]. Nickel-cadmium ferrite oxide is widely used in many technological and applications such as magnetic disks, receiver antenna, induction coils, microwave absorbing devices, core transformers. The ferrite nonmaterial can be synthesized by various chemical methods such as double sintering ceramic method [10], co-precipitation [11], hydrothermal [12] Sol-gel [13], Oregano-metallic precursor [14], citrate precursor [15], gel auto-combustion [16], etc.

The sol-gel technique has been utilized effectively to produce high-quality nanocrystalline spinel ferrites with specific properties such as better homogeneity, lower preparation temperatures, relatively shorter processing times, high purity of materials, improved material properties, and reduced cost [13]. This method involves the oxidation/reduction reaction of aerogel, which is obtained from an aqueous solution consisting of desired metal salts (oxidizers) and organic complexant (reductant). During aerogel combustion, the quick growth of a large volume of gases leads to the formation of nanoparticles. Also, the line intensity of the in-field gives strong evidence for a ferromagnetic structure up to x=0.30 composition. The cations distribution and physicochemical properties of Ni-Cd ferrite nanoparticles by employing a citrate gel process same result observed by Lohar et al. [17]. They confirmed that the Ni-Cd samples are suitable material for the recording heads and antenna rods application due to its soft magnetic behavior. The magnetic properties ferrites will be improved by substituting the other metal ions into the host lattice. $Cd^{2+}$ is a nonmagnetic ion and a very capable candidate in them.

In my research article, the composite of Nickel Cadmium ferrite is a co-mixed spinel structure wherein the concentration of cadmium can modify the magnetic behaviors. Besides, the dielectric properties are also important properties concerning applications at high frequencies. Our best knowledge, very less work found in literature has been reported on the dielectric properties of Ni-based Cd ferrites. However, some works on dielectric properties of Ni–Zn, Ni-Cd, and Mn–Zn ferrites have been reported [18-20]. Taken together; the major strengths of the present work are twofold. First, we employed gel auto combustion route to synthesized $Ni_{1-x}Cd_xFe_2O_4$ (x = 0.0 to 0.5) ferrite samples. Second, we have analysis of the structural, magnetic, dielectric constant with dielectric loss of the cadmium-substituted nickel ferrites.

## 2. EXPERIMENTAL PROCEDURE

Samples of $Ni_{1-x}Cd_xFe_2O_4$ (X=0.0 to 0.5) were prepared by the sol-gel auto combustion route. A mixture of chemical composition solution prepared in double-distilled water $Fe(NO_3)_3.9H_2O$, with $Ni(NO_3)_2.6H_2O$ and $Cd(NO_3)_2.6H_2O$ in an appropriate proportion was taken. The prepared chemical composition solution was stirred continuously at 3 hr on a magnetic stirrer to get a uniform combination. Further, the glycine solution (fuel) was slowly added into the obtained chemical combinations due to the formation of a redox mixture. The solution was then dehydrated gradually onto a hot plate with continuous stirring then the sticky gel was formed. Further, the prepared sticky gel at a particular temperature auto-explosion (fire) of the black ash and finally gets fluffy gel took place in the beaker. The obtained powder was grinded for 40 min and sintered at the 1000$^o$C for 6 h in a programmable auto furnace. Then the powder is hard-pressed into the pellets by using a 4% PVA binder and by applying pressure of near about 6 ton for 6 min. These pellets were finally sintered at 1100$^o$C for 10 hr to reduce porosity, the present PVA binder vaporized, and increase density. These prepared samples were further used for studying structural, electrical, magnetic, and dielectric properties

## 3.CHARACTERIZATION TECHNIQUES:

The structural properties were studied by Bruker D2-Phaser X-ray diffractometer (XRD) with Cu-Kα radiation (λ=1.5406 Å). The surface morphology was carried out using a Field emission scanning electron microscope (FESEM)(Mira-3, Tescan, Brno-Czech Republic). The DC electrical resistivity was estimated by utilizing the two probe meter with highly sensitive Keithley electrometer model-6514. The Fourier transform infrared spectra (FTIR) were recorded in the range 360–1000 $cm^{-1}$ at room temperature using the Alpha-100508 spectrometer was. The magnetic properties of all samples were explored using a vibrating sample magnetometer (VSM) Lakeshore-7000 model. The dielectric measurements were carried out using a high precision LCR meter bridge model-HP-6284A in the frequency range 20Hz to 1MHz.

## 4. RESULTS AND DISCUSSION

### 4.1 X-RAY DIFFRACTION STUDY

The structural analysis of these prepared sample ferrites ($Ni_{1-x}Cd_xFe_2O_4$) were carried out by using X-ray diffraction technique on Rigaku, diffractometer (Cu Kα radiation, $\lambda$ =1.540562Å, 2Ø= 20–80°). Fig.1. shows the lattice peak are (111), (220), (222), (311), (400), (422), (511), and (440). It indicates that the formation of spinel cubic structure similarly results observed by M. De et.al [21]. It is also seen that the intensity of the peak lattice planes decreases with an increase in $Cd^{2+}$concentration due to no other reflections peaks are observed in all samples.

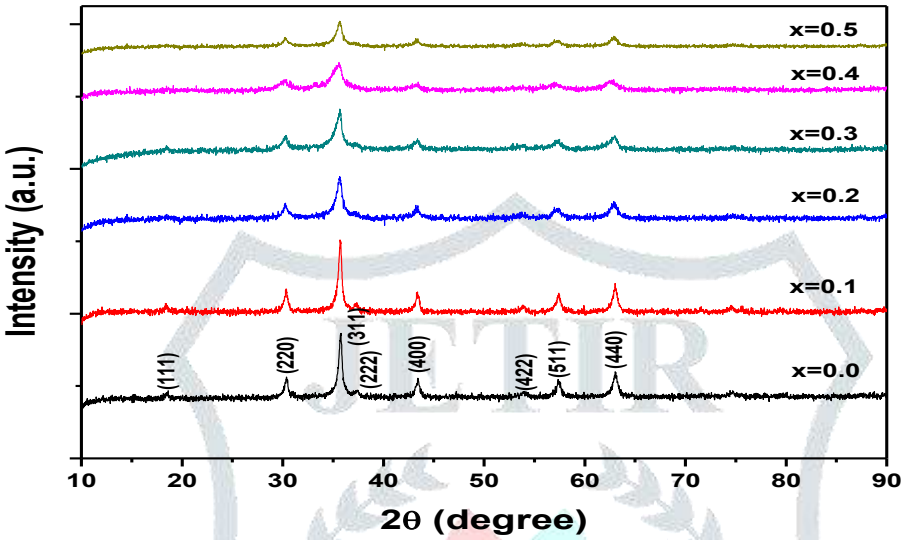


**Fig. 1.** X-ray diffraction patterns of $Ni_{1-x}Cd_xFe_2O_4$ (x=0.0 to 0.5) ferrite system

In fig.1 clearly shows the (311) peak position is slightly shifted towards the lower angle side due to the linear increase in the lattice constant upon increasing $Cd^{2+}$ content which is the observed result match with good agreement with Vegard's law[22]. The crystallite size (*D*) was estimated from the XRD peak broadening of the lattice peak (311) by using Debye Scherrer's relation [23].

$$D=\frac{0.9*\lambda}{\beta cos\emptyset} \quad (1)$$

Where, $k$ = 0.9 is the Scherrer's constant, $\lambda$ =1.540562Å is the wavelength of X-rays and $\beta$ is the full-width half maxima (FWHM) of the lattice peak at an angle. The average crystallite size (*D*) has been calculated using Scherer's formula given as 42.8 nm,38.6 nm,35.5nm,33.2 nm,31.2 nm, and 29.8 nm for the $Cd^{2+}$(0.0% to 0.5%) doped nickel ferrite. The crystallite size increases with increasing $Cd^{2+}$ content in nickel ferrite due to $Cd^{2+}$ ions occupies A-sites. The lattice constant of all samples were determined by using the formula [24].

$$a = d\sqrt{h^2 + k^2 + l^2} \quad (2)$$

Where, '*a*' is the lattice constant, (hkl) represents the Miller indices and d represents the interplanar distance. The values of lattice constant (*a*) increased with increasing $Cd^{2+}$ content in nickel ferrite. The observed values of lattice constant are in good agreement with those reported in the literature [25]. The tetrahedral and octahedral bond lengths $R_A$, $R_B$, and ionic radii $r_A$, $r_B$ of the samples are calculated by using XRD data and depicted in similarly relation used Hemant Kumar Dubey et.al[13]. Table 1. The bond lengths $R_A$, $R_B$, and ionic radii $r_A$, $r_B$ of A-site and B-site was increased linearly due to the increase in lattice constant concerning $Cd^{2+}$ content.

### 4.2 FIELD EMISSION SCANNING ELECTRON MICROSCOPY

Fig.2.the micrographs of prepared $Ni_{1-x}Cd_xFe_2O_4$ ferrite samples by auto combustion route analyzed by using FE-SEM microscopy. The samples contained cotton cluster-like structures. The existence of cotton clusters in the synthesized nanoparticles may be recognized as the magnetic dipole interaction with the nearby nanoparticles. It is evident from FE-SEM investigation that

the grain of nickel cadmium ferrite is in nanoscale with striking pores. The voids and mesopores present in the examples could be recognized for the release of gases during the explosion process.

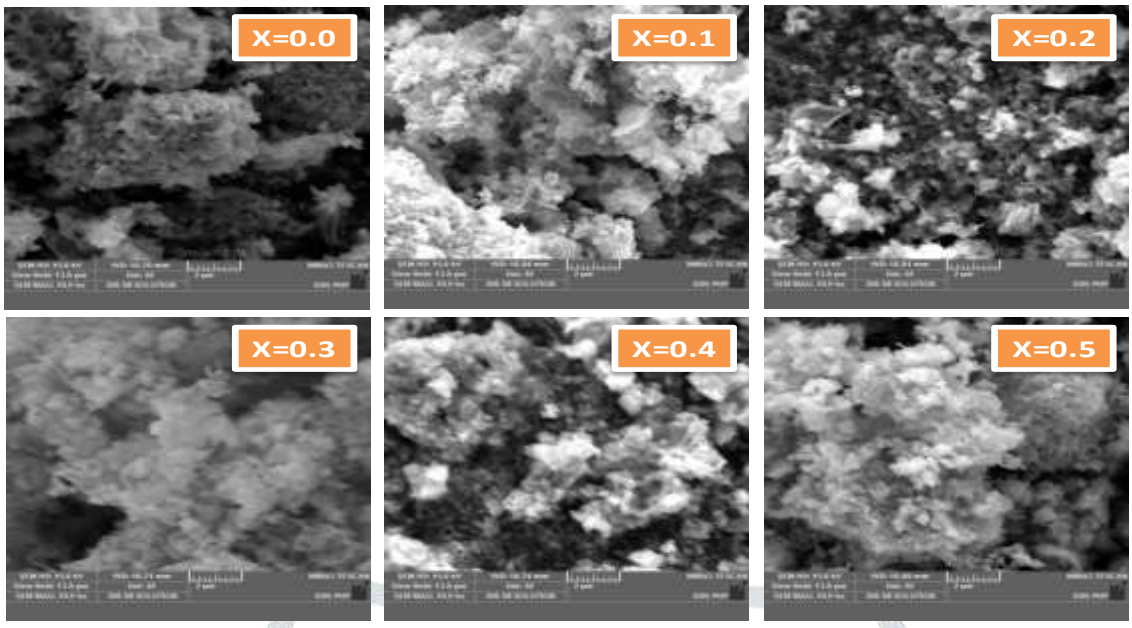


**Fig.2.** FESEM images of $Ni_{1-x}Cd_xFe_2O_4$ (x=0.0 to 0.5) ferrite system

From the micrographs, one can particularly see that the morphological changes occur with varying Cd content (x) in $Ni_{1-x}Cd_xFe_2O_4$. In the few samples with x = 0.0 and 0.5, one can see that the grains are very much isolated. By addition of $Cd^{2+}$ the grain size increases along with a packet of the cotton spheres. The average particle size of the ferrite system was found to be 0.5–1.0 μm. The observed disparity in grain size is accredited to the grain-growth mechanism involving diffusion coefficients and the concentration of dissimilar ions. Besides, we utilized the energy-dispersive X-ray(EDAX) spectroscopy, which is used to investigate the chemical composition for the constituent elements of the synthesized nanomaterials. The EDAX result (Fig.3) confirmed the presence of elements Ni, Cd, Fe, and O without any impurity. The atomic weight % of major elements presented inside the EDAX spectra corroborates the formation of Ni-Cd ferrite.

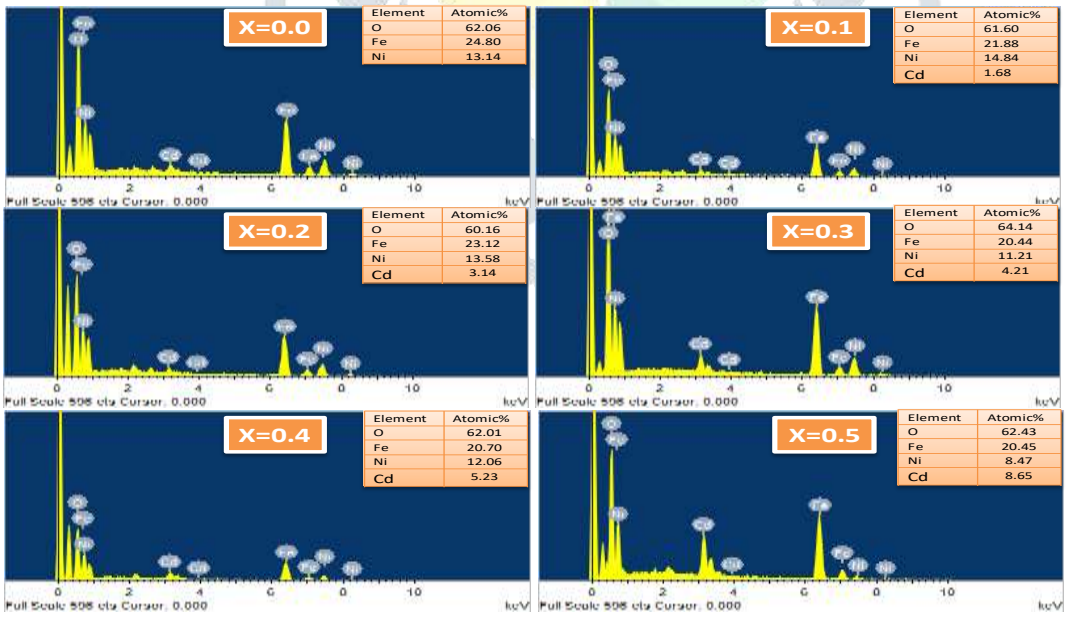


**Fig. 3.** EDAX spectra of $Ni_{1-x}Cd_xFe_2O_4$ (x=0.0 to 0.5) ferrite system

### 4.3 FTIR ANALYSIS

To validate the formation of spinel structure and to look at the chemical properties of the material, the infrared (IR) spectroscopy of $Cd^{2+}$ substituted nickel ferrite was carried out. The analysis of IR spectra can give information about the structural modification and to get information about the position of cations in the spinel lattice. The IR spectra of $Ni_{1-x}Cd_xFe_2O_4$ (x=0.0 to 0.5) ferrite system is shown in Fig. 4. The spectra show the two strong characteristic absorption bands in the range of about 600 to 400$cm^{-1}$. The highest concentrated band is observed at about 586 $cm^{-1}$ ($\upsilon_1$) which correspond to intrinsic stretching vibrations of the metal ions and oxygen at the tetrahedral A-site as well as lowest band is observed at about 394 $cm^{-1}$ ($\upsilon_2$) which correspond to metal-oxygen stretching vibrations of octahedral B-site[26].

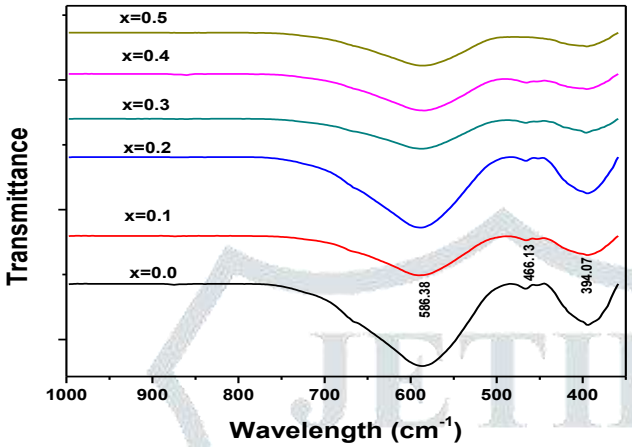


**Fig. 4.** FTIR spectra of $Ni_{1-x}Cd_xFe_2O_4$ (x=0.0 to 0.5) ferrite system

When $Cd^{2+}$ content in the nickel ferrite was increases as the result the highest band is transferred towards a higher frequency side and but the position of the lowest band does not much change. It takes place due to the larger ionic radii of $Cd^{2+}$ than $Ni^{2+}$ ions at octahedral A-site, the $Cd^{2+}$ ion occupies only the tetrahedral A-sites and it remains constant at the interstitial A-sites, this leads to an increase in the highest band towards higher frequency side. Similar IR spectra of the metal ion substituted nickel ferrite were reported in Pachpinde et.al[27]. The slight variation in the position and intensities of the highest absorption bands is due to the difference in the $Fe^{3+}$-O and $Cd^{2+}$-O distances from A-sites. The divergence in the band position is predictable because of the difference in the $Fe^{3+}$-$O^{2-}$ distances for the octahedral A-sites. The distinction in lattice constant and cation distribution is responsible for the band shift of the center frequency. The increase in the unit cell dimensions due to the replacement of $Ni^{2+}$ ions by $Cd^{2+}$ ions affects the $Ni^{2+}$-$O^{2-}$ stretching vibration which causes the change in higher band position. The varying in the frequency of the $\upsilon_1$ stretching band shows that the first choice of $Cd^{2+}$ ions and occupies the tetrahedral A-sites.

### 4.4. DC ELECTRICAL RESISTIVITY

The DC electrical resistivity of the materials is a paramount property cognate of the materials utilized in the fabrication of electronic contrivances. The nickel ferrite is considered to be a high resistive spinel ferrite material [28].

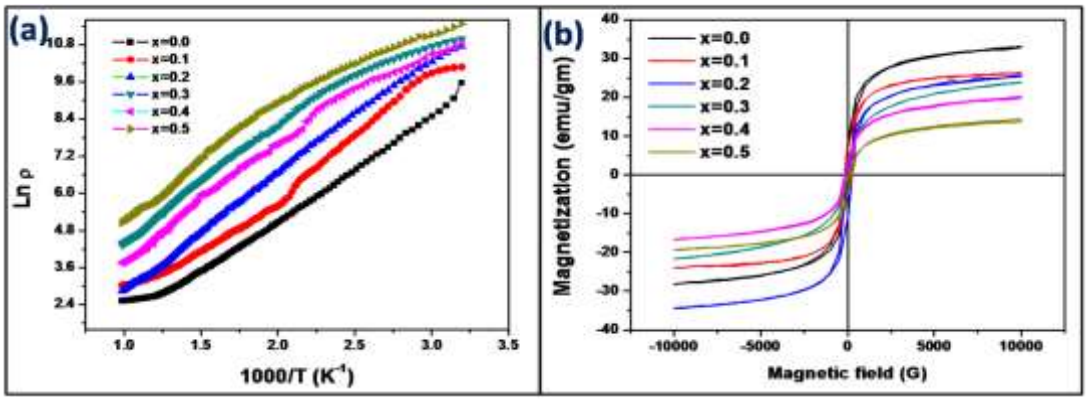


**Fig. 5(a).**DC electrical resistivity with temperature **(b)**M-H curves of $Ni_{1-x}Cd_xFe_2O_4$ (x=0.0 to 0.5) ferrite system measured at room temperature

The DC resistivity of ferrite material could be enhancing after doping the trivalent or divalent ion and the first choice of the occupying ion to fill the A-sites or B-sites. The DC electrical resistivity exhibits temperature dependence of $Ni_{1-x}Cd_xFe_2O_4$ (x=0.0 to 0.5) ferrite system is shown in Fig.5(a) it follows the exponential relationship i.e. the Arrhenius plot. For all samples, linear reduction in resistivity with an increase in temperature which demonstrated the semiconducting character. The decrease resistivity of the $Ni_{1-x}Cd_xFe_2O_4$ with an increase in temperature may be due to an increase in the thermally activate mobility of charge carriers, according to the charges hopping conduction mechanism [26/21]. The DC resistivity graph shows the two temperature regions and their slopes will be different. At lower temperatures, the first region is observed due to the ordered state of ferromagnetic nature and at the higher temperature, the second region is observed which is due to electron hopping or disordered paramagnetic nature. The activation energy (ΔE) was calculated in two temperature regions, i.e., ferromagnetic and paramagnetic region, and is tabulated in Table 1.

| $Cd^{2+}$ Content (x) | Lattice constant a (Å) | Crystallite size D (nm) | rA ($A^0$) | rB ($A^0$) | $R_A$ ($A^0$) | $R_B$ ($A^0$) | Activation energy,ΔE (eV) | | Curie temperature Tc ($^oC$) |
|---|---|---|---|---|---|---|---|---|---|
| | | | | | | | Ferromagnetic region | Paramagnetic region | |
| 0.0 | 8.3214 | 45 | 1.8881 | 2.031 | 0.5381 | 0.6804 | 0.24 | 0.28 | 615 |
| 0.1 | 8.3421 | 49 | 1.8928 | 2.033 | 0.5428 | 0.6854 | 0.28 | 0.35 | 597 |
| 0.2 | 8.3549 | 58 | 1.8957 | 2.039 | 0.5457 | 0.6885 | 0.26 | 0.37 | 589 |
| 0.3 | 8.3616 | 63 | 1.8972 | 2.041 | 0.5472 | 0.6902 | 0.33 | 0.35 | 581 |
| 0.4 | 8.3692 | 66 | 1.8989 | 2.043 | 0.5489 | 0.692 | 0.22 | 0.30 | 575 |
| 0.5 | 8.3739 | 72 | 1.9011 | 2.044 | 0.550 | 0.6932 | 0.38 | 0.39 | 550 |

**Table.1.**Lattice constant, crystallite size, ionic radii, bond length, activation energy and Curie temperature of $Ni_{1-x}Cd_xFe_2O_4$ (x=0.0 to 0.5) ferrite system

It is noted from the table that the activation energies of the paramagnetic region are higher than the ferromagnetic region due to disordering states [29] and are in good conformity with the theory of Irkin and Turor et.al [30]. Also, the activation energy increase is confirmed that the barriers energy increase for hopping electrons, these results show increasing the DC electrical resistivity. The Curie temperature (*Tc*) of the ferrite system varies from 550 to 615 °C as shown in Table 1. In ferrite materials, all of the values of *Tc* depend on the existence of a cations and bond strength of the A-site and B-site. In nickel ferrite, the $Ni^{2+}$ ions are replaced by $Cd^{2+}$ ions hence increase in the strength of the A-B interaction without change in B-site $Fe^{3+}$ ions. Therefore, the values of Curie temperature decrease with an increase in $Cd^{2+}$ content in nickel ferrites. The conduction below Curie temperature is due to the hopping of electrons between $Fe^{2+}$ and $Fe^{3+}$ ions, whereas, above Curie temperature, the conduction is due to the polarons hopping [31]. The decreases in Curie temperature (*Tc)* for increase in $Cd^{2+}$substitution for other spinel ferrite was observed by Lohar et al. [17]

**4.5 MAGNETIC PROPERTIES**

Fig.5 (b). shows the room temperature M-H hysteresis curves of $Ni_{1-x}Cd_xFe_2O_4$ (x=0.0 to 0.5) ferrite system. The observed magnetic parameters from hysteresis curves are presented in Table 2. A variation in saturation magnetization and coercivity was observed with an increase in $Cd^{2+}$ concentration. This can be attributed to the superexchange interactions between the divalent metal ions and $Fe^{3+}$ ions in the octahedral B-site in the spinel lattice. The net magnetization in ferromagnetic substance was dependent not only on type but also on the number of ions located at the tetrahedral (A) and octahedral (B) sites because this distribution affects the magnetizations, $M_S$, and $H_C$ of the A and B sub-lattices, respectively. The loss of magnetization from x = 0.0 to x =0.5 with $Cd^{2+}$ substitution might be due to the replacement of $Ni^{2+}$ by $Cd^{2+}$ with which in turn descend the resultant net magnetic moment.

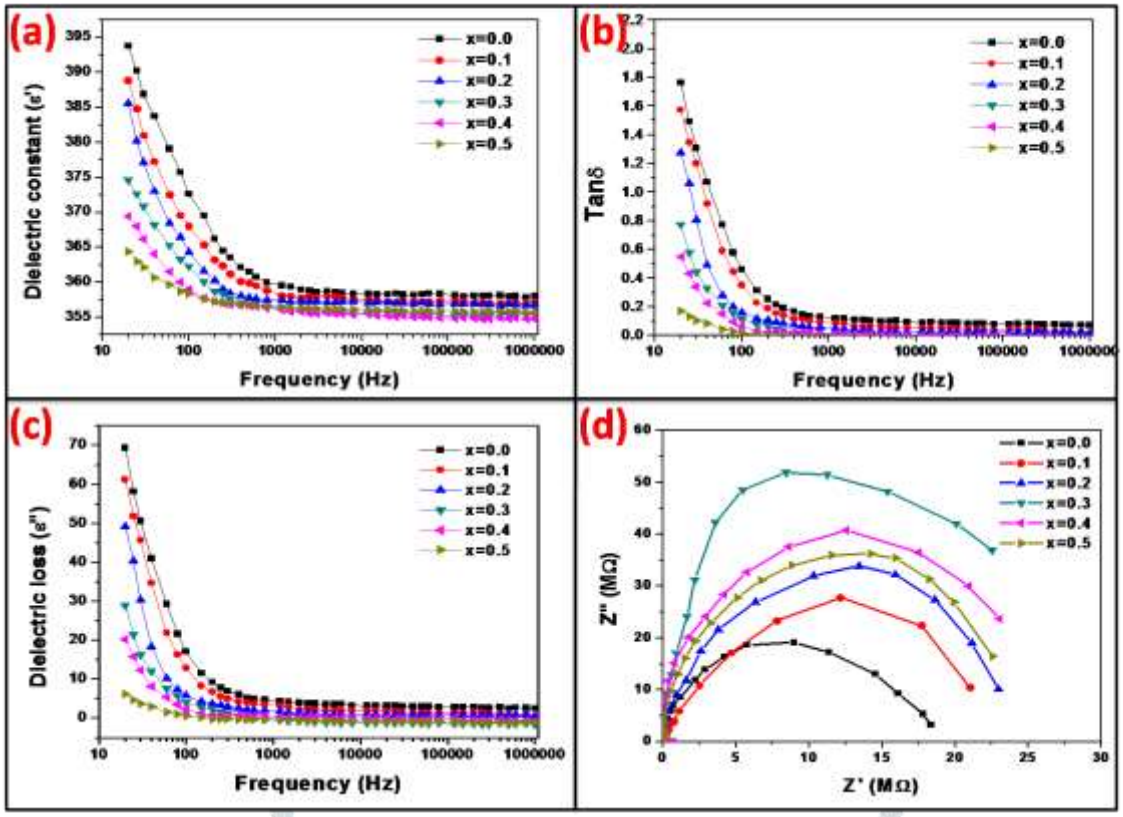


**Fig. 6.(a)** Real part of dielectric constant with frequency **(b)** Dielectric loss tangent (tanδ) with frequency **c)** Imaginary part of dielectric constant with frequency **d)** Nyquist plots of $Ni_{1-x}Cd_xFe_2O_4$ (x=0.0 to 0.5) ferrite system

Also, the decrease in the magnetization is might be due to the quenching of the total orbital momentum leaving the spins to the only effective parameter. So, one can expect that the larger $Cd^{2+}$ ions will prefer to occupy tetrahedral A-sites. When the $Cd^{2+}$ substitution increased, the saturation magnetization reduced as compared with the pure nickel ferrite. It is due to the fact that nonmagnetic $Cd^{2+}$ ions (0 μB) replace magnetic $Ni^{2+}$ ions (2 μB) [32]. $Cd^{2+}$ ions are highly non-magnetic; thus the ferromagnetic region decreases at the expense of the paramagnetic region by replacing $Ni^{2+}$ ions. The total magnetic moments in the ferrite spinel completely based on the number of magnetic ions fill in the tetrahedral and octahedral sites [33]. Also, the increasing crystallite size with an increase in $Cd^{2+}$ ions leads to the increase of random spins which causes the reduction of magnetization. Since $Cd^{2+}$ is a non-magnetic ion, it doesn't participate in the exchange interactions with its nearest atom. Therefore, the magnetic super-exchange interaction between the $Cd^{2+}$ and $Ni^{2+}$cations decreases with the increase of concentration [34]. The lower value of the coercive field is observed for the composition x=0.2 composition. This can be attributed to the change in magneto-crystalline anisotropy due to the substitute of $Ni^{2+}$ ions by $Cd^{2+}$ ions from the A-site. After that, the coercive field (Hc) increases with $Cd^{2+}$ content, it may occur due to the increasing crystallite size with an increase in $Cd^{2+}$ content. For bulk particles coercivity and crystallite size have reciprocal relation [35]. The small coercive field predicts that it can be used in high-density data storage devices because minimum coercivity allows writing and overwriting of data. In the present study, the variation of coercivity (Hc) and crystallite size (D) correlated with each other, and the coercivity which was found to be in the range of 73-256G. Also, the maximum value of the coercivity was seen for the composition with x=0.0 which has crystallite size 45 nm while the minimum value of the coercivity was found to be for the composition at x=0.2 having crystallite size 58 nm. The coercivity of ferromagnetic ferrite depend on metal ions entering into the interstitial sites of spinel lattice, which may distort the lattice and generate an internal stress and the nonmagnetic ions have a strong spin-orbit coupling [36]. Therefore, the samples having coercivity Hc > 600 Oe was suitable for the application of magnetic recording media, and the samples of coercivity in the range 600-900 are suitable for switching circuit, sensor, and high microwave frequency applications [37].

| $Cd^{2+}$ content (x) | Cation Distribution | Ms (emu/gm) | Mr (emu/gm) | Hc (G) | Mr/Ms | Anisotropy constant $K\times10^{3}$ (erg/g) |
|---|---|---|---|---|---|---|
| 0.0 | $(Fe_1^{+2})[Ni_1^{2+}Fe_1^{3+}])O_4^{-2}$ | 33.12 | 8.51 | 253 | 0.256 | 8.7 |
| 0.1 | $(Cd_{0.1}^{2+}Fe_{0.9}^{+2})[Ni_{0.9}^{2+}Fe_{1.1}^{3+}])O_4^{-2}$ | 26.30 | 6.26 | 216 | 0.238 | 5.9 |
| 0.2 | $(Cd_{0.2}^{2+}Fe_{0.9}^{+2})[Ni_{0.8}^{2+}Fe_{1.1}^{3+}])O_4^{-2}$ | 25.69 | 1.43 | 73 | 0.040 | 1.9 |
| 0.3 | $(Cd_{0.3}^{2+}Fe_{0.9}^{+2})[Ni_{0.7}^{2+}Fe_{1.1}^{3+}])O_4^{-2}$ | 23.88 | 2.28 | 114 | 0.095 | 2.8 |
| 0.4 | $(Cd_{0.4}^{2+}Fe_{0.9}^{+2})[Ni_{0.6}^{2+}Fe_{1.1}^{3+}])O_4^{-2}$ | 20.09 | 3.10 | 165 | 0.154 | 3.4 |
| 0.5 | $(Cd_{0.5}^{2+}Fe_{0.9}^{+2})[Ni_{0.5}^{2+}Fe_{1.1}^{3+}])O_4^{-2}$ | 14.26 | 2.77 | 101 | 0.194 | 1.5 |

**Table. 2.** Cation distribution and magnetic parameter of $Ni_{1-x}Cd_xFe_2O_4$ (x=0.0 to 0.5) ferrite system

The anisotropy constant (K) will depend on the $Cd^{2+}$ ion concentration, which can be determined by using the well-known relation [38] and values are presented in Table 2. The magnetic anisotropy of the material is directly proportional to the coercivity and variation is occurred with increasing $Cd^{2+}$ content. The shape and region of the curve are directly associated with grain size, density, porosity, and chemical composition that in turn are influenced by annealing condition.

**4.6 DIELECTRIC PROPERTIES**

The dielectric properties such as real and imaginary part of dielectric constant (ε') and loss tangent (tanδ) of all samples are studied in the frequency range 20 Hz to 1 MHz. The real part of the dielectric constant (ε') was estimated using the equation [39].

$$\varepsilon' = \frac{C_p t}{\varepsilon_0 A} \qquad (3)$$

Where Cp is capacitance, t is thickness, A is be the area of the cross-section of the synthesized pellet and $\varepsilon_0$ is the permittivity of free space. Fig.6(a) shows the discrepancy of real part of dielectric constant (ε') with frequency in Hz of $Ni_{1-x}Cd_xFe_2O_4$ (x=0.0 to 0.5) system. The real part of the dielectric constant linearly decreases at a low-frequency region and it remains constant at a higher frequency region which indicates the common type of dielectric dispersion. This dielectric dispersion is also accredited to Maxwell–Wagner type [40, 41] polarizations included between the slid faces; this exhibits good agreement with Koop's theory [42]. The decrease in ε' at low frequencies due to at some frequencies electric charge can't follow the changes of applied electric field and electron hopping between $Fe^{3+}$ and $Fe^{2+}$ ions in the ferrite materials. Due to the occurrence of $Fe^{3+}$ and $Fe^{2+}$ ions ferrite is termed as dipolar behavior. The dipoles create rotational displacement results in the orientation of polarization. The rotation of $Fe^{2+}\leftrightarrow Fe^{3+}$ dipoles can be fantastically as the exchange of ions so that the alignment of dipoles generates a response to the applied alternating electric field [43]. In Ni-Cd ferrite, the $Ni^{2+}$ ions present in tetrahedral A-site are responsible for decreasing in concentration of $Fe^{3+}$ ions in octahedral B-site which reduces the movement of $Fe^{2+}$ to $Fe^{3+}$. Therefore at lower frequency region the ε' decreases and attains constant at the higher frequency side. The similar effect of dielectric constant with applied frequency of nickel ferrite was observed by Belavi et.al[44]. Fig.6(b) shows the variation of loss tangent (tanδ) with frequency and showing the similar trend of ε'. It is seen that at a lower frequency region the loss tangent is maximum and then decreases and remains constant at higher frequencies due to domain wall movement is upturned by the rotational movement of dipoles [45]. The electrical resistivity and dielectric dispersion in ferrite spinel are may be due to the interchange mechanism along with charge carriers at an A-site and B-site ions [46]. The dielectric constant of the prepared materials exhibits inversely proportional to square root of resistivity. The imaginary element of dielectric constant (ε") is estimated as the relation, ε"=ε'tanδ where as tan δ is be the tangent dielectric loss, these tangent dielectric loss shows that the function of energy loss between the applied electric field and prepared ferrite sample. Fig.6(c) shows the different imaginary element of dielectric constant (ε") vs frequency of the Ni-Cd ferrite. The effect of annealing of temperature, addition of the impurities, and structural homogeneity of materials shows on the dielectric constant (ε") [47]. The dielectric losses are exhibits well supported to dominant of resonance at ferrite materials. The higher frequency range shows very less dielectric losses, it may be due to dominant motion and rotations of dipoles are changed by magnetic force [13]. The conduction mechanism of ferrite is studied by using complex impedance spectroscopy of the Ni-Cd ferrite

system is shown in Fig.6(d). The electrochemical impedance spectroscopy (EIS) indicate that the real (Z') vs imaginary (Z") parts, EIS shows incomplete semicircles may due to the material possesses high resistance at lower frequencies. The diameter of the semicircle is varied with $Cd^{2+}$ content in nickel ferrite due to the increase in the grain interior resistance of the material.

## 5. CONCLUSIONS

Nanostructured $Ni_{1-x}Cd_xFe_2O_4$ (x=0.0 to 0.5) ferrite system was successfully synthesized by employing a solution combustion route. The XRD analysis revealed that all the prepared samples are single-phase cubic spinel crystal structure without any additional phase. The increases in lattice constant and an increase in crystallite size shows that the expansion of the unit cell may be due to different ionic radii. The SEM confirmations that all ferrite material samples exhibit an exaggerated continuous grain growth with grains containing some fine pores. FTIR confirmed that the presence of two main characteristic absorption bands, corresponding to the vibration of the tetrahedral and octahedral sites respectively. The study of DC electrical resistivity confirms that the semiconductor nature of ferrite materials. The activation energies of the paramagnetic region are higher than the paramagnetic region and the Curie temperature (*Tc*) decreases from 615 to 550°C with an increase in $Cd^{2+}$ content. The magnetic behavior of $Cd^{2+}$ substituted nickel ferrite shows soft ferromagnetic nature. The saturation magnetization (Ms) and coercivity (Hc) were decreased with increase $Cd^{2+}$ content be due to the increase of disordered spins which reduces the exchange interaction between tetrahedral and octahedral sites. The dielectric measurements for all the ferrite material sample shows a usual dielectric dispersion may be due to occurs space charge polarization. The impedance spectroscopy chemical analysis suggests a grain internal role in the conduction process.

## 6.CONFLICT OF INTERESTS

Authors declare that they have no conflicts of interests.

## REFERENCES

[1] Teber A, Cil K, Yilmaz T, et al. Manganese and zinc spinel ferrites blended with multi-walled carbon nanotubes as microwave absorbing materials.Aerospace. 2017;4:2–18.

[2] J.M. Grenche, J. Teillet, H. Pascard, A mixed nickel-cadmium ferrite investigated by Mösbauer spectrometry,J. Magn. Magn. Mater. 140-144 (1995) 2087-2088, https://doi.org/10.1016/0304-8853(94)01395-0.

[3] G. A. Sawatzky, F. Van Der Woude, A. H. Morrish, Mössbauer Study of Several,Ferrimagnetic Spinels,Phys. Rev. 187 (1969) 747-757,DOI:https://doi.org/10.1103/PhysRev.187.747.

[4]S.Singhal,S.Jauhar,N.Lakshmi,S.Bansal,$Mn^{3+}$ substituted Co–Cd ferrites, $CoCd_{0.4}Mn_xFe_{1.6-x}O_4$ ($0.1 \leqslant x \leqslant 0.6$): Cation distribution, structural, magnetic and electrical properties, J. Mol. Struct. 1038 (2013) 45–51. https://doi.org/10.1016/j.molstruc.2013.01.020

[5] C. Upadhjay, D. Mishra, H.C. Varma, S. Anaud, R.P. Das, Effect of Preparation Conditions on Formation of Nanophase Ni-Zn Ferrites Through Hydrothermal Technique, J. Magn. Magn. Mater. 260 (2003) 188-194. DOI: 10.1016/S0304-8853(02)01320-3

[6] S.E. Shirsath, B.G. Toksha, K.M. Jadhav, Structural and magnetic properties of In3+ substituted NiFe2O4,Mater. Chem. Phys. 117 (2009) 163-168. https://doi.org/10.1016/j.matchemphys.2009.05.027

[7] S.M. Patange, S.E. Shirsath, S.S. Jadhav, K.M. Jadhav, Cation distribution study of nanocrystalline $NiFe_{2-x}Cr_xO_4$ ferrite by XRD, magnetization and Mössbauer spectroscopy Phys. Status Solidi A 209 (2012) 347-352, https://doi.org/10.1002/pssa.201127232.

[8] S.Hua, H. Zhang, X. Tang, X. Xiang, High-permeability and high-Curie temperature NiCuZn ferrite,J. Magn. Magn. Mater. 283 (2004) 157-163 DOI: 10.1016/j.jmmm.2004.05.017

[9] H. Zhong, H. Zhang, Effects of different sintering temperature and Mn content on magnetic properties of NiZn ferrites, J. Magn. Magn. Mater. 283 (2004) 247-250, https://doi.org/10.1016/j.jmmm.2004.05.029..

[10] S.E. Shirsath, S.S. Jadhav, B.G. Toksha, S.M. Patange, K.M. Jadhav, Influence of $Ce^{4+}$ ions on the structural and magnetic properties of $NiFe_2O_4$, J. Appl. Phys. 110 (2011) 013914, https://doi.org/10.1063/1.3603004.

[11] S.M. Patange, S.E. Shirsath, B.G. Toksha, S.S. Jadhav, K.M. Jadhav, Electrical and magnetic properties of Cr3+ substituted nanocrystalline nickel ferrite,J. Appl. Phys. 106 (2009) 023914, https://doi.org/10.1063/1.3176504

[12] Wang Z, Xie Y, Wang P, et al. Microwave anneal effect on magnetic properties of Ni0.6Zn0.4Fe2O4 nanoparticles,prepared by conventional hydrothermal method. J Magn Magn Mater. 2011;323:3121–3125.

[13] Hemant Kumar Dubey , Preeti Lahiri Synthesis, structural, dielectric and magnetic properties of $Cd^{2+}$ based Mn nanosized ferrites, Materials Technology, (2020), DOI:10.1080/10667857.2020.1734728.

[14] T.T. Srinivassan, P. Ravindranathan, L.E. Cross, R. Ray, Studies on high-density nickel-zinc ferrite and its magnetic properties using novel hydrazine precursors, J. Appl. Phys. 63 (1988) 3789, https://doi.org/10.1063/1.340615

[15] Y. Atassi, M. Tally, Low sintering temperature of Mg-Cu-Zn ferrite prepared by the citrate precursor method,J. Iranian Chem. Soc. 3 (2006) 242-246.

[16] S.E. Shirsath, R.H. Kadam, A.S. Gaikwad, A. Ghasemi, A. Morisako, Effect of sintering temperature and the particle size on the structural and magnetic properties of nanocrystalline $Li_{0.5}Fe_{2.5}O_4$, J. Magn. Magn. Mater. 323 (2011) 3104-3108, https://doi.org/10.1016/j.jmmm.2011.06.065.

[17] K.S. Lohar, S.M. Patange, M.L. Mane, Sagar E. Shirsath, Cation distribution investigation and characterizations of $Ni_{1-x}Cd_xFe_2O_4$ nanoparticles synthesized by citrate gel process, J. Mol. Struct. 1032 (2013) 105-110, https://doi.org/10.1016/j.molstruc.2012.07.055.

[18] Bhagwat S, Rao P. Study of dielectric properties of nano-crystalline Mn-Zn Ferrite. J Appl Phys.2013;3:01–06.

[19] Verma A, Goel TC, Mendiratta RG, et al. Dielectric properties of NiZn ferrites prepared by the citrate precursor method. Mater Sci Eng B. 1999;60:156–162.

[20] Devmunde BH, Raut AV, Birajdar SD, et al.Structural, electrical, dielectric, and magnetic properties of Cd2+ substituted nickel ferrite nanoparticles,J Nanoparticles. 2016;8:1–8.

[21] M. De, A. Mukherjee, H.S. Tewari, Characterization of cadmium substituted nickel ferrites prepared using auto-combustion technique, Processing and Application of Ceramics 9 (2015) 193-197, https://doi.org/10.2298/PAC1504193D.

[22] C.G. Winfrey, D.W. Eckart, A. Tauber, "Preparation and X-ray diffraction data for some rare earth stannets,J. Am. Chem. Soc. 82 (1960) 2695–2697.

[23]A.L. Jadhav, S.V. Kambale, R.M. Kore, B.J. Lokhande,Capacitive Study of Nickel Oxide Thin Films Prepared by Spray Pyrolysis,International Journal of Fracture and Damage Mechanics 5 (2)(2019), 17-22.

[24] A. V. Raut, R. S. Barkule, D. R. Shengule, K.M. Jadhav, Synthesis, structural investigation and magnetic properties of $Zn^{2+}$ substituted cobalt ferrite nanoparticles prepared by the sol–gel auto-combustion technique,J. Magn. Magn. Mater. 358-359 (2014) 87–92, https://doi.org/10.1016/j.jmmm.2014.01.039.

[25] Y.L. Huang, W.B. Fan, Y.H. Hou, K.X. Guo, Y.F. Ouyang, Z.W. Liu, Effects of intrinsic defects on the electronic structure and magnetic properties of CoFe 2 O 4 : A first-principles study, J. Magn. Magn. Mater., 429 (2017) 263-269, https://doi.org/10.1016/j.jmmm.2017.01.043.

[26] V.S. Sawant, A.A. Bagade, S.V. Mohite, K.Y. Rajpure, Studies on structural and electrical properties of $Li_{0.5-0.5x}Co_xFe_{2.5-0.5x}O_4$ ($0 \le x \le 0.6$) spinel ferrite,Physica B. 474, (2015) 47-52, https://doi.org/10.1016/j.physb.2015.06.005.

[27] A.M. Pachpinde, M.M. Langade, K.S. Lohar, S.M. Patange, S.E. Shirsath, Impact of larger rare earth $Pr^{3+}$ ions on the physical properties of chemically derived $Pr_xCoFe_{2-x}O_4$ nanoparticles,Chem. Phys. 429 (2014) 20-26, https://doi.org/10.1016/j.chemphys.2013.11.018.

[28] R. Ahmad, I.H. Gul, M. Zarrar, H. Anwar, M.B.K. Niazi, A. Khan, Improved electrical properties of cadmium substituted cobalt ferrites nano-particles for microwave application

,J. Magn. Magn. Mater. 405 (2016) 28-35, https://doi.org/10.1016/j.jmmm.2015.12.019.

[29] A. Dais, R.L. Moreira, Conductivity behavior of *n*-type semiconducting ferrites from hydrothermal powders, J. Mater. Res. 12 (1998) 2190, DOI: https://doi.org/10.1557/JMR.1998.0306.

[30] Y.P. Irkin, E.A. Turor, Sovt. Phys. JEPT. 33 (1957) 673.

[31] D. Ravinder, B. Ravi Kumar, Electrical conductivity of cerium substituted Mn–Zn ferrites

,Mater. Lett. 57 (2003) 1738-1742, DOI: 10.1016/S0167-577X(02)01060-1.

[32] Gopathi Ravi Kumar, Katrapally Vijaya Kumar, Yarram Chetty VenudharSynthesis, Structural and Magnetic Properties of Copper Substituted Nickel Ferrites by Sol-Gel MethodA. Goldman, Modern Ferrite Technology, Van Nostrand Reinhold Company, New York, NY, USA, 1990.

[33] R.N. Panda, J.C. Shih, T.S. Chin, Magnetic properties of nano-crystalline Gd- or Pr-substituted $CoFe_2O_4$ synthesized by the citrate precursor technique,J. Magn. Magn. Mater. 257 (2003) 79-86, https://doi.org/10.1016/S0304-8853(02)01036-3.

[34] L. Kumar, M. Kar, Ceram. Int. Effect of $La^{3+}$ substitution on the structural and magnetocrystalline anisotropy of nanocrystalline cobalt ferrite ($CoFe_{2-x}La_xO_4$),38 (2012) 4771-4782, https://doi.org/10.1016/j.ceramint.2012.02.065.

[35] V.R.K. Murthy, B. Viswanathan, Ferrite Materials, Narosa Publishing House, 1990.

[36] Y. Wang, F. Xu, L. Li, H. Liu, H. Qiu, Magnetic properties of La-substituted Ni–Zn–Cr ferrites via rheological phase synthesis, J. Jiang, Mater. Chem. Phys. 112 (2008) 769-773. https://doi.org/10.1016/j.matchemphys.2008.06.032

[37] M. Ahmad, I. Ali, R. Grössinger, M. Kriegisch, F. Kubel, M.U. Rana, J. Alloys Compnd. 579 (2013) 57-64.

[38] S.S. Jadhav, S.E. Shirsath, S.M. Patange, K.M. Jadhav, Effect of Zn substitution on magnetic properties of nanocrystalline cobalt ferrite, J. Appl. Phys. 108 (2010) 093920-093926. https://doi.org/10.1063/1.3499346

[39] S.R. Kulkarni, C.M. Kanamadi, B.K. Chougule, Dielectric and magnetoelectric properties of (x)Ni{sub 0.8}Co{sub 0.1}Cu{sub 0.1}FeâOâ/(1 - x)PbZr{sub 0.8}Ti{sub 0.2}Oâ composites,

Mater. Res. Bull. 40 (2005) 2064-2072 , DOI: 10.1016/j.materresbull.2005.07.014

[40] J.C. Maxwell, Electricity and Magnetism, Vol. 1. Oxford University Press, New York, (1973) 88.

[41] K.W. Wagner, Am. Phys. 40 (1973) 817-819.

[42] C.G. Koops, On the Dispersion of Resistivity and Dielectric Constant of Some Semiconductors at Audiofrequencies,Phys. Rev. 83 (1951) 121-124, DOI:https://doi.org/10.1103/PhysRev.83.121.

[43] A.A. Bagade, K.Y. Rajpure, Studies on $NO_2$ gas sensing properties of sprayed $Co_{1-x}Mn_xFe_2O_4$ ($0 \leq x \leq 0.5$) spinel ferrite thin films,Ceram. Int. 41 (2015) 7394-7401, https://doi.org/10.1016/j.ceramint.2015.02.051.

[44] P.B. Belavi, G.N. Chavan, L.R. Naik, R. Somashekar, R.K. Kotnala, Structural, electrical and magnetic properties of cadmium substituted nickel–copper ferrites,Materials Chemistry and Physics 132 (2012) 138-144, https://doi.org/10.1016/j.matchemphys.2011.11.009.

[45] F. Muthafar, L. Sean, K.S. Kassim, Structural analysis, magnetic and electrical properties of samarium substituted lithium–nickel mixed ferrites, J. Magn. Magn. Mater. 324 (2012) 873-879, https://doi.org/10.1016/j.jmmm.2011.10.005.

[46] S.P. Yadav, S.S. Shinde, A.A. Kadam, K.Y. Rajpure, Structural, morphological, dielectrical and magnetic properties of Mn substituted cobalt ferrite,J. Semicond. 34 (2013) 093002.

[47] S.S. Bellad, B.K. Chougle, Composition and frequency dependent dielectric properties of Li–Mg–Ti ferrites, Mater. Chem. Phys. 66 (2000) 58-63, https://doi.org/10.1016/S0254-0584(00)00273-X.